Published in final edited form as:
Dev Cell. 2014 November 24; 31(4): 487–502. doi:10.1016/j.devcel.2014.09.013.

The chromosome axis controls meiotic events through a hierarchical assembly of HORMA domain proteins

Yumi Kim[1,4], **Scott C. Rosenberg**[2,4], **Christine L. Kugel**[2,3], **Nora Kostow**[1], **Ofer Rog**[1], **Vitaliy Davydov**[2], **Tiffany Y. Su**[2], **Abby F. Dernburg**[1,5], and **Kevin D. Corbett**[2,5]

[1]Department of Molecular and Cell Biology, University of California, Berkeley, CA 94720-3220, USA; Howard Hughes Medical Institute, 4000 Jones Bridge Road, Chevy Chase, MD 20815, USA; Department of Genome Dynamics, Life Sciences Division, Lawrence Berkeley National Laboratory, Berkeley, CA 94720, USA; California Institute for Quantitative Biosciences, Berkeley, CA 94720, USA

[2]Ludwig Institute for Cancer Research, San Diego Branch, Department of Cellular and Molecular Medicine, University of California, San Diego, La Jolla, CA 92093-0660, USA

Summary

Proteins of the HORMA domain family play central but poorly understood roles in chromosome organization and dynamics during meiosis. In *C. elegans*, four such proteins (HIM-3, HTP-1, HTP-2, and HTP-3) have distinct but overlapping functions. Through combined biochemical, structural, and *in vivo* analysis, we find that these proteins form hierarchical complexes through binding of their HORMA domains to cognate peptides within their partners' C-terminal tails, analogous to the "safety belt" binding mechanism of Mad2. These interactions are critical for recruitment of HIM-3, HTP-1, and HTP-2 to chromosome axes. HTP-3, in addition to recruiting the other HORMA domain proteins to the axis, plays an independent role in sister chromatid cohesion and double-strand break formation. Finally, we find that mammalian HORMAD1 binds a peptide motif found both at its own C-terminus and that of HORMAD2, indicating that this mode of intermolecular association is a conserved feature of meiotic chromosome structure in eukaryotes.

[3]Present address: University of California, San Francisco, 513 Parnassus Avenue, San Francisco CA 94143, USA
[4]Co-first author.
[5]Co-senior author. Contact: KDC (kcorbett@ucsd.edu), AFD (afdernburg@lbl.gov)

Author Contributions

YK, SCR, KDC, and AFD planned the experiments. YK prepared samples for mass spectrometry and analyzed the data, performed reconstitution experiments, prepared mutant *C. elegans* strains, analyzed phenotypes, and performed immunofluorescence imaging, assisted by NK. SCR performed reconstitution experiments, determined crystal structures, and performed peptide binding assays. CLK performed co-expression tests with mutant peptide-HORMA complexes. OR generated plasmids and mutant *C. elegans* strains. VD and TS purified human HORMAD proteins and performed the pulldown. KDC, AFD, YK, and SR wrote the manuscript.

Introduction

Meiosis is the specialized cell division program in which homologous chromosomes, and then sister chromatids, segregate from one another in two successive divisions to generate haploid gametes. The emergence of this process during evolution required major innovations in chromosome organization and function. A ubiquitous feature of meiosis is the formation of chromosome axes, which organize replicated chromosomes into linear arrays of DNA loops (Blat et al., 2002; Zickler and Kleckner, 1999). These axes form the lateral elements of the tripartite synaptonemal complex (SC), which mediates stable interhomolog juxtaposition (synapsis) (Kleckner, 2006; Zickler and Kleckner, 1999). Axis assembly is essential for homologous pairing and synapsis, and is also required for proper initiation and regulation of meiotic recombination (Panizza et al. 2011; Niu 2005; Schwacha and Kleckner 1997). The axis comprises meiosis-specific cohesin complexes and, in most species, proteins of the HORMA domain family.

The HORMA domain was first recognized by sequence similarity in three functionally diverse budding yeast proteins: Hop1, the fungal meiotic chromosome axis protein; Rev7, an accessory subunit of the translesion DNA polymerase ζ; and the spindle assembly checkpoint protein Mad2 (HORMA: Hop1/Rev7/Mad2) (Aravind and Koonin, 1998). More recently, HORMA domains have been characterized in the Mad2 regulator $p31^{comet}$ and the autophagy factor Atg13 (Jao et al., 2013; Xia et al., 2004; Yang et al., 2007). The best-studied HORMA domain protein, the spindle checkpoint protein Mad2, binds and inhibits Cdc20 to prevent APC/C activation and anaphase onset until kinetochores are attached to spindle microtubules. Mad2 undergoes a conformational change from an “open” to a “closed” conformation when it binds to short peptides within Cdc20 or Mad1, a kinetochore adaptor for Mad2 (Luo et al., 2002; 2004; Sironi et al., 2002). Through dimerization with closed Mad2 at the kinetochore, soluble open Mad2 switches to the closed conformation to become an active, diffusible Cdc20 inhibitor. Currently, it remains unclear whether other HORMA domain proteins share these properties of conformational switching and binding partner exchange.

Throughout eukaryotic phyla, the meiosis-specific HORMA domain proteins localize to the chromosome axis, which is established during early meiotic prophase. There they promote double-strand DNA break (DSB) formation by Spo11/SPO-11 (Goodyer et al., 2008; Panizza et al., 2011), bias recombination toward the homolog to promote crossover formation (Martinez-Perez and Villeneuve, 2005; Niu et al., 2005; Schwacha and Kleckner, 1997), mediate homolog pairing and SC assembly (Daniel et al., 2011; Hollingsworth et al., 1990; Wojtasz et al., 2009), and participate in meiotic checkpoints that monitor synapsis and/or crossover formation (Baumgartner et al., 2000; Wojtasz et al., 2012). Fungi have a single meiosis-specific HORMA domain protein (Hop1) (Hollingsworth and Johnson, 1993) while mammals and plants express two paralogs (HORMAD1/2 and ASY1/2, respectively) (Caryl et al., 2000; Chen et al., 2005; Fukuda et al., 2010; Pangas et al., 2004; Wojtasz et al., 2009), and the nematode *C. elegans* has four (Couteau and Zetka, 2005; Goodyer et al., 2008; Hodgkin et al., 1979). The four meiotic HORMA domain proteins in *C. elegans* (HIM-3, HTP-1, HTP-2, and HTP-3) have related but distinct functions. HTP-3 is required for axis localization of HIM-3, HTP-1, and HTP-2 (Goodyer et al., 2008; Severson et al.,

2009), and its absence leads to failures in sister chromatid cohesion, homolog pairing, synapsis, and DSB formation (Goodyer et al., 2008). HIM-3 is dispensable for axis localization of cohesins and HTP-3, but is required for homolog pairing and synapsis (Couteau et al., 2004; Zetka et al., 1999). HIM-3 also promotes crossover formation by biasing recombination to the homolog instead of the sister chromosome, reflecting a function conserved in fungal and mammalian HORMA domain proteins (Couteau and Zetka, 2011; Couteau et al., 2004; Martinez-Perez and Villeneuve, 2005; Niu et al., 2005; Schwacha and Kleckner, 1997; Shin et al., 2010; Wojtasz et al., 2009; 2012; Zetka et al., 1999). Finally, HTP-1 and HTP-2 are highly similar to one another and appear to play partially overlapping roles. While *htp-2* mutants have no obvious meiotic defects, *htp-1* mutants exhibit extensive nonhomologous synapsis, suggesting a role in restricting SC assembly to occur between properly paired homologs (Couteau and Zetka, 2005; Martinez-Perez and Villeneuve, 2005), while loss of both paralogs results in severe abrogation of synapsis. These proteins also play a role in defining the pattern of cohesin removal during the meiotic divisions. In *C. elegans*, the single crossover site on each holocentric chromosome defines two distinct regions, a “short arm” where cohesion is released during meiosis I and “long arm” that retains cohesion until meiosis II (Kaitna et al., 2002; Nabeshima et al., 2005; Rogers et al., 2002). While HTP-3 and HIM-3 persist along both arms, HTP-1 and HTP-2 become restricted to the long arms in late prophase (Martinez-Perez et al., 2008) mirroring the localization of LAB-1, a direct protector of cohesin complex integrity (de Carvalho et al., 2008; Tzur et al., 2012).

Despite their wide conservation and fundamental roles in meiosis, how the HORMA domain proteins interact with each other to establish the meiotic chromosome axis and to govern chromosome dynamics during meiosis is unknown. Here we combine *in vitro* reconstitution, X-ray crystallography, and *in vivo* analysis of mutant proteins to reveal that the *C. elegans* meiotic HORMA domain proteins associate with one another through specific binding of each protein’s HORMA domain with short motifs, which we designate as “closure motifs,” in the proteins’ C-terminal tails. The resulting hierarchical assemblies of HORMA domain proteins are critical for the assembly of the chromosome axis, formation of the SC, and the faithful segregation of chromosomes in meiosis.

Results

The structure of HIM-3 reveals a conserved C-terminal “closure motif”

To establish the molecular basis for meiotic HORMA domain protein function, we sought to determine these proteins’ 3D structures. The four *C. elegans* meiotic HORMA domain proteins share a similar domain structure, with an N-terminal HORMA domain and a variable-length C-terminal tail predicted to lack intrinsic structure, ranging from ~50 residues in HIM-3 to ~100 residues in HTP-1 and HTP-2, and over 500 residues in HTP-3.

We first crystallized and determined the 3D structure of full-length HIM-3 to a resolution of 1.75 Å (Table 1). Residues 19-248 (of 291) of HIM-3 adopts a HORMA domain fold, consisting of a seven-stranded β-sheet backed on one side by three long α-helices (Figure 1A). This structure is extremely similar to those of Mad2 and Rev7 in their “closed” conformations (Figure S1A). The most significant structural difference between HIM-3 and

previously characterized HORMA domain proteins is an extended loop between β5 and αC (residues 127-158 in HIM-3), which drapes over the β-sheet and forms an additional short α-helix not observed in Mad2 or Rev7. This loop is intimately associated with the C-terminal β-strands β8′ and β8″ through both ionic and Van der Waals interactions, potentially stabilizing HIM-3 in the closed state (see below).

In the closed states of Mad2 and Rev7, a peptide ligand forms a β-strand that packs against strand β6 of the HORMA domain and is held in place by a "safety belt" encompassing β-strands β7, β8′, and β8″ (Hara et al., 2010; Luo et al., 2002; Sironi et al., 2002). In our structure of HIM-3, experimental electron density maps clearly revealed a peptide forming a β-strand apposed to β6. The high resolution of our structure enabled us to unambiguously identify this peptide as residues 278-286 of HIM-3 (Residues ~249-277 are disordered in our structure; Figure 1, S3A). Because HIM-3 adopts a closed conformation around this C-terminal motif, we designate it the HIM-3 "closure motif".

Sequence alignments of HIM-3 orthologs in related nematodes revealed that the HIM-3 closure motif is highly conserved, particularly a Pro-Tyr-Gly motif that is closely associated with the "safety belt" of the HORMA domain in our structure (Figure 1B,C, S1B). We also identified a similar conserved motif near the C-termini of HTP-1 and HTP-2 and their orthologs, which contains a nearly invariant Pro-Tyr-Ser motif (Figure 1C, S1C). The long C-terminal tail of HTP-3 has a repetitive sequence in which six motifs bearing signatures of the HIM-3 closure motif can be discerned (Figure 1C). Four of these motifs (#2-5) are nearly identical to one another, and flanking these four motifs are two variable motifs (#1 and 6), with motif #6 located at the extreme C-terminus of HTP-3. Sequence alignments of HTP-3 orthologs from related nematodes reveal only limited sequence homology outside the HORMA domain, but we were able to identify potential closure motifs in the C-termini of HTP-3 orthologs from *C. briggsae*, *C. remanei*, *C. brenneri*, *C. japonica*, and *C. sp. 5* (Figure S1D).

C. elegans meiotic HORMA domain proteins form intermolecular complexes

The identification of several putative "closure motifs" within the tail of HTP-3, together with the knowledge that HTP-3 is required for association of the other meiotic HORMA domain proteins with the axis, suggested that axis assembly might be mediated by HORMA domain:closure motif interactions. To test this idea, and to identify other components associated with the *C. elegans* meiotic chromosome axis, we purified HTP-3-containing protein complexes from a worm strain expressing a functional *htp-3-gfp* fusion (*ieSi6*). Mass spectrometry analysis of soluble HTP-3 complexes indicated that the protein physically associates with HIM-3, HTP-1, and HTP-2 (Figure 2A). A parallel analysis of chromosome-associated HTP-3 complexes additionally detected multiple cohesin subunits, including the meiosis-specific kleisin subunits REC-8, COH-3, and COH-4 (Figure 2A). These results indicate that *C. elegans* axial elements are mainly composed of cohesin complexes and the four meiotic HORMA domain proteins, consistent with prior genetic and cytological studies (Couteau and Zetka, 2005; Goodyer et al., 2008; Martinez-Perez and Villeneuve, 2005; Zetka et al., 1999).

To investigate how the four HORMA domain proteins interact with one another, we used a bacterial polycistronic expression system to co-express various combinations of the four proteins. When expressed individually, both HIM-3 and HTP-3 were soluble and monomeric in solution, as judged by size exclusion chromatography and multi-angle light scattering (SEC-MALS) (Figure 2B, C, S2). HTP-1 formed soluble aggregates when expressed on its own (not shown), but when HTP-1 was co-expressed with HIM-3 we detected soluble complexes with a stoichiometry of 1 HIM-3:1 HTP-1 (Figure 2B, C). Co-expression of HIM-3, HTP-1, and HTP-2 yielded a mixture of 1 HIM-3:1 HTP-1 and 1 HIM-3:1 HTP-2 complexes (not shown).

When HTP-3 was co-expressed with different combinations of HIM-3, HTP-1, and HTP-2, the resulting complexes were heterogeneous. Analysis of the composition and average molecular weights of these complexes indicated that multiple copies of the smaller HORMA domain proteins can associate simultaneously with a single HTP-3 (Figure 2, S2). Importantly, we found that HTP-1 and HIM-3 could each associate independently with HTP-3 (Figure 2C). Together, these results reveal that HTP-3 is able to associate simultaneously with multiple copies of HIM-3, HTP-1, and HTP-2.

Specific HORMA domain-closure motif interactions define a hierarchical assembly

Our reconstitution experiments showed that HIM-3, HTP-1, and HTP-2 can each bind directly to HTP-3, and that HTP-1 and HTP-2 can also independently bind HIM-3. By co-expressing truncated proteins, we further found that the HIM-3:HTP-1 interaction requires the C-terminal tail of HIM-3 (co-expression of HTP-1 with HIM-3 (1-245) did not result in a complex despite expression of both proteins; not shown), and also required the HORMA domain of HTP-1, but not its C-terminal tail. These results strongly suggest that the HIM-3-HTP-1 interaction is mediated by HORMA domain-closure motif binding *in trans* (Figure 2B; compare measured stoichiometry of HTP-1:HIM-3 with HTP-1 (1-253):HIM-3). Using a fluorescence polarization (FP) peptide-binding assay, we measured the affinity and specificity of HORMA domain:closure motif interactions. We found that HIM-3 binds strongly to a peptide that includes the HTP-3 motif #4 sequence (K_d 0.3 μM; Figure 3A), and is therefore likely to also bind motifs #2, #3, and #5. However, HIM-3 did not bind a randomized version of HTP-3 motif #4, nor did it bind the divergent HTP-3 motifs #1 or #6. As full-length HIM-3 was used for this binding assay, our results show that HTP-3 motif #4 can effectively compete for binding to the HORMA domain of HIM-3 in the presence of the closure motif within HIM-3's tail. By contrast, full-length HIM-3 did not effectively bind in *trans* to the motif found within its own tail. To further characterize the selectivity of the HIM-3 HORMA domain, we co-expressed untagged HIM-3 HORMA domain (residues 1-245) in *E. coli* together with tagged closure motif peptides and measured HIM-3 association using a pulldown assay. In this assay, the HIM-3 HORMA domain bound strongly to HTP-3 motif #4, but again did not detectably bind its own closure motif (not shown). Together with results from the FP peptide-binding assay described above, this indicates that binding of the HORMA domain of HIM-3 to the closure motif within its own tail is a low-affinity interaction that depends on the high effective concentration imparted by covalent association between the HORMA domain and tail.

We next measured the binding of HTP-1 and HTP-2 to various closure motif peptides (Figure 3B,C). As noted above, both HTP-1 and HTP-2 form soluble aggregates when expressed in isolation, and the resulting purified proteins did not specifically bind any peptides in the FP assay (not shown). However, co-expression of His_6-tagged HTP-1 or HTP-2 with untagged HTP-3 resulted in a mixed population of HTP-3:HTP-1/2 complexes and free monomeric HTP-1/2, suggesting that HTP-3 may act as a chaperone for these proteins when they are co-expressed in *E. coli*. When these monomers were purified away from their respective HTP-3 complexes, both HTP-1 and HTP-2 bound strongly to the HIM-3 closure motif and to HTP-3 motifs #1 and #6, but did not associate detectably with HTP-3 motif #4 (Figure 3B,C). The two proteins showed similar specificities, with only subtle differences in binding affinities (Figure 3D).

Full-length HTP-3 did not detectably associate with either the HIM-3 or HTP-2 closure motif peptides in our peptide-binding assay (not shown). In co-expression/pulldown tests, the HTP-3 HORMA domain was also unable to interact with any of the identified closure motifs in its own C-terminus (not shown); we were unable to confirm this result through peptide binding assays due to the difficulty in purifying the truncated HTP-3 construct. Overall, these results are consistent with the idea that HTP-3 binds an as-yet-unidentified partner to mediate its localization to the meiotic chromosome axis.

Finally, none of the four proteins associated with the putative closure motif at the C-terminus of HTP-2. Notably, this motif and that of HTP-1 contain a serine in place of the highly conserved glycine in other closure motifs; our *in vitro* and *in vivo* data (see below) suggest that larger amino acid side chains at this position might interfere with binding. It is possible that the highly-conserved C-terminal motifs in HTP-1 and HTP-2 act as low-affinity closure motifs that facilitate HTP-1/2 folding or stability, but evidence supporting this idea is currently lacking. Taken together, our peptide binding assays are consistent with the knowledge that HIM-3, HTP-1, and HTP-2 require HTP-3 to associate with the meiotic chromosome axis, and suggest that that they are recruited to the axis by binding of their HORMA domains to specific closure motifs within HTP-3 and/or HIM-3 (Figure 3E).

Specific closure motifs within HTP-3 recruit HIM-3 to mediate homologous synapsis

To gain insight into the functional importance of the interaction between HIM-3 and HTP-3, we determined the structure of a chimeric protein in which the closure motif of HIM-3 was replaced by HTP-3 motif #4. This structure shows the HIM-3 HORMA domain in essentially the same conformation as in the native HIM-3 structure (Cα r.m.s.d. of 0.62 Å over 228 residues), and shows strong electron density for residues 649-662 of HTP-3 (Figure 4A, B, S3B) within the binding pocket. The interaction of the HIM-3 HORMA domain with HTP-3 motif #4 is much more extensive than with its own closure motif, burying 1620 $Å^2$ of total surface area versus 1150 $Å^2$ for the intramolecular binding interaction, consistent with the higher affinity measured in our peptide-binding and pull-down assays. HTP-3 residues 650-654 adopt a β-strand conformation and form a continuous β-sheet with HIM-3 β6 (within the HORMA domain) and β7 (in the “safety belt”). The tyrosine residue conserved in all closure motifs (Y651 in HTP-3 motif #4) is positioned close to the HIM-3 safety belt, and makes a hydrogen bond with asparagine 139 of HIM-3.

The following residue, glycine 652, is buried against the HIM-3 HORMA domain. Arginine 653, conserved in HTP-3 motifs #2-5, makes a salt bridge with HIM-3 glutamate 115. This arginine residue is conserved in the majority of closure motifs we identified in *Caenorhabditis* HTP-3 orthologs (Figure S1D), and glutamate 115 is highly conserved in *Caenorhabditis* HIM-3 orthologs; this interaction may therefore represent a specific feature of HTP-3:HIM-3 complexes. The C-terminus of the closure motif (HTP-3 residues 657-662) forms an amphipathic α-helix that packs against a hydrophobic cavity in the HIM-3 HORMA domain. The hydrophobic residues in this helix are conserved within HTP-3 motifs #2-5, but in motifs #1 and #6 the corresponding side chains are charged or polar. Thus, several distinct features of HTP-3 closure motifs #2-5 contribute to HIM-3's preference for these sequences.

In all of our HORMA domain:closure motif structures, a conserved glycine near the N-terminus of the closure motif is packed tightly against a hydrophobic surface in the HORMA domain (Figure 4B,C). We found that mutation of this glycine to lysine in HTP-3 motif #4 (G652K) abolished binding to HIM-3 in two independent *in vitro* assays (Figure 4D, S4A). We therefore created HTP-3^{4GK}, in which the conserved glycine residues in the four central HTP-3 closure motifs (#2-5) were all mutated to lysine. As expected, this 4GK mutation strongly abrogated binding of HIM-3 to HTP-3 when the proteins were co-expressed in *E. coli*, but did not affect binding of HTP-1 to HTP-3 (Figure 4E). This result agrees with our peptide binding data, and validates the idea that HTP-3 motifs #2-5 are specific binding sites for HIM-3.

To determine the consequences of disrupting HIM-3:HTP-3 binding *in vivo*, we engineered an *htp-3-gfp* transgene with the 4GK substitutions, which was used to generate transgenic animals by Mos1-mediated single copy insertion (MosSCI) (Frøkjaer-Jensen et al., 2008) at a defined genomic locus (ttTi5605 on Chr II). Worms expressing either wild-type or 4GK mutant HTP-3-GFP were crossed to the null allele *htp-3(tm3655)*. The wild-type *htp-3-gfp* transgene supported normal chromosome axis and SC assembly dynamics (Figure 4F-H) and fully rescued the viability of embryos produced by homozygous animals (100% of embryos from *htp-3(tm3655) I; htp-*3^{WT} *II* were viable, compared to 13% from *htp-3*(*tm3655) I*) (Figure S4C, D). HTP-3^{4GK}-GFP showed slightly lower protein expression compared to the wild-type tagged protein (Figure S4B), but localized properly to the chromosome axes in meiotic nuclei (Figure 4F). However, animals expressing HTP-3^{4GK}-GFP produced mostly dead eggs (only 3.1% of embryos produced by self-fertilizing *htp-3(tm3655) I; htp-*3^{4GK} *II* survived to adulthood), and 27.5% of the few survivors were males (Figure 4F, S4C, D), indicating that mutation of these central four motifs leads to severe defects in meiotic chromosome segregation. Consistent with our *in vitro* data, HIM-3 failed to load onto the chromosomes in the HTP-3^{4GK} mutant, while HTP-1 was still detected along the axes (Figure 4F). As in *him-3* mutants, chromosomes failed to pair and synapse in the HTP-3^{4GK} mutant (Figure 4G, H). These results demonstrate that HTP-3 closure motifs #2-5 play a critical role in chromosome axis assembly and homolog synapsis through their recruitment of HIM-3 to the chromosomes. The localization of HTP-1 to the chromosomes in the HTP-3^{4GK} mutant further confirms that HTP-1/HTP-2 recruitment can be mediated by direct binding to HTP-3, presumably through motifs #1 and #6, in the absence of HIM-3.

Redundant mechanisms recruit HTP-1 and HTP-2 to the meiotic chromosome axis

The HIM-3 HORMA domain binds specifically to HTP-3 closure motifs #2-5. In contrast, HTP-1 and HTP-2 preferentially bind to HTP-3 motifs #1 and #6, and bind the HIM-3 closure motif with similarly high affinity (Figure 3B-D). To determine the basis for their specificity, we co-expressed and purified the HORMA domains of both HTP-1 and HTP-2 (residues 1-253 of 352) with different closure motifs. HTP-2 readily co-crystallized with the HIM-3 motif, HTP-3 motif #1, and HTP-3 motif #6, and we determined structures for each of these complexes (Figure 5D-G, Table 1). When initial crystallization screens for HTP-1:closure motif complexes failed, we examined the crystal packing interactions of HTP-2 complexes. Based on this analysis, we designed a point mutant of HTP-1 (proline 84 to leucine, P84L) to mimic a specific crystal packing interaction observed in HTP-2 structures. This residue resides on a surface-exposed α-helix (αB) and is poorly conserved among HTP-1/HTP-2 orthologs, so this mutation is unlikely to have a significant effect on HTP-1's structure or binding. Complexes containing the mutant HTP-1(1-253)^{P84L} crystallized readily in conditions similar to those for HTP-2(1-253) complexes, and we determined its structure bound to both the HIM-3 closure motif and HTP-3 closure motif #1 (Figure 5A-C).

HTP-1 and HTP-2 share 82% sequence identity, and their HORMA domains have nearly identical crystal structures, with an overall Cα r.m.s.d of less than 0.5 Å (Figure 5A, D). Both are also highly similar to HIM-3 (~1.0 Å r.m.s.d between 180 aligned Cα atoms), with most of the differences in flexible loop regions. The residues that form the closure motif binding pockets within HTP-1 and HTP-2 are identical, and their modes of interaction with closure motifs are also virtually indistinguishable (e.g. compare Figure 5B and E). The highly conserved Tyr-Gly pair within the closure motifs adopts an identical conformation in all HTP-1/2 structures, tightly engaged by strand β7 of the associated HORMA domain's "safety belt". The major difference when compared to HIM-3 is the conformation of the C-terminal portion of the bound closure motifs: while a HIM-3-bound closure motif adopts a short amphipathic α-helix (Figure 4B), all three motifs that bind HTP-1 and HTP-2 adopt a β-strand conformation at both ends of the motif, with a small bulge in the middle (Figure 5). This bulge is one residue longer in HTP-3 motif #1 than in the other two motifs, but otherwise the three motifs are bound by the HTP-1 HORMA domain in a nearly identical manner (compare Figure 5E with 5F and 5G; alignment in Figure 5H). Each of these three motifs also possesses an arginine N-terminal to the conserved Tyr-Gly pair that packs into the same negatively charged pocket on the HORMA domain, despite variation in its position within each closure motif . Other interactions in the HTP-1 and HTP-2 complexes are mostly backbone-backbone hydrogen bonds characteristic of β-sheets, providing little sequence specificity. This is reminiscent of Mad2, whose known binding peptides in Cdc20, Mad1, and Shugoshin bear only weak sequence similarity (Luo et al., 2002; Orth et al., 2011).

We next generated disruptive glycine-to-lysine mutations in HTP-3 motifs #1 and #6 (motif #1, G490K; motif #6, G728K; both, 2GK), and tested for binding by HIM-3 or HTP-1 when co-expressed in *E. coli*. None of these mutations affected HIM-3 binding (Figure 5I), while HTP-1 binding was clearly affected: Mutation of HTP-3 motif #1 (G490K) alone

significantly reduced HTP-1 binding. Unexpectedly, mutation of motif #6 (G728K) had no detectable effect on HTP-1 binding, yet did appear to synergize with mutation of motif #1, since the HTP-3^{2GK} mutant did not detectibly bind to HTP-1 (Figure 5I). This suggests that HTP-1 interacts more strongly with HTP-3 motif #1 than #6, consistent with results from our peptide binding assays (Figure 3B, C). Together with our peptide binding and structural data, these results confirm that HTP-3 motifs #1 and #6 are specific binding sites for HTP-1 and HTP-2.

We next introduced these same mutations (HTP-3 motif #1 (G490K), motif #6 (G728K), and the double mutant (2GK)) into worms by MosSCI and crossed each transgene to the *htp-3(tm3655)* null allele to test the roles of these motifs in meiotic chromosome axis assembly and synapsis. Surprisingly, all three mutant transgenes supported high levels of embryonic viability (G490K, 96.1%; G728K, 100%; 2GK, 98.6%). Consistent with this, in each of these mutants, HTP-1/2 and HIM-3 were detected at the meiotic chromosome axis (Figure 5J, S5A), and robust homologous synapsis was observed, albeit with a modest delay in animals expressing HTP-3^{G490K} or HTP-3^{2GK} (Figure 5K, S5B, C). Because the double mutant (HTP-3^{2GK}) protein failed to bind HTP-1 *in vitro* (Figure 5I), we reasoned that axis localization in this mutant is likely mediated through binding of HTP-1/2 to HIM-3, which in turn is recruited by HTP-3. Consistent with this, when HTP-3^{2GK} was crossed into the *him-3(gk149)* null background, HTP-1/2 was drastically reduced on meiotic chromosomes, and chromosome synapsis was eliminated (Figure 5J, K). Similar results were observed when all six closure motifs within HTP-3 were mutated (HTP-3^{6GK}), which eliminated recruitment of HIM-3, HTP-1, and HTP-2 (Figure 5J, K). Notably, we found that animals expressing a truncated HIM-3 protein lacking the closure motif (residues 1-245) were proficient to recruit HTP-1/2 to the chromosome axis and showed no meiotic nondisjunction (Figure S5A). Taken together, these results indicate that HTP-1/2 can be recruited to the axis by binding to HTP-3 motifs #1 and #6, or by binding to the closure motif within HIM-3, and that either mode of HTP-1/2 recruitment is sufficient to support homologous synapsis and meiotic chromosome segregation.

HTP-3 promotes chromosome cohesion and DSB formation, independent of HIM-3 and HTP-1/HTP-2 recruitment to the meiotic chromosome axis

In addition to promoting homolog pairing and synapsis and double-strand break formation, HTP-3 is required to maintain sister chromatid cohesion until meiosis II (Severson et al., 2009). Our evidence that HTP-3 recruits the other HORMA domain proteins to the axis through motifs in its C-terminal tail enabled us to test whether these roles of HTP-3 require the other HORMA domain proteins. To determine how HTP-3 contributes to cohesion, we compared cohesin loading in *htp-3* null mutants vs. animals expressing the engineered HTP-3^{6GK} variant, which shows normal axis association but fails to recruit HIM-3 and HTP-1/2. In wild-type animals, cohesin complexes containing the common SMC subunits SMC-1 and SMC-3, but with distinct kleisin subunits (REC-8 or COH-3/COH-4), localize along meiotic chromosome axes from meiotic entry through late pachytene (Pasierbek et al., 2001; Severson et al., 2009). While SMC-1, SMC-3 and COH-3/COH-4 were detected on chromosomes in two *htp-3* null mutants (*tm3655* and *y428*; data not shown for *y428*) (Figure 6B, S6A, B), REC-8 staining was greatly diminished (Figure 6A), as previously reported

(Severson et al., 2009). By contrast, REC-8 was clearly retained on meiotic chromosomes in HTP-3^{6GK} mutants (Figure 6A). These results indicate that HTP-3 promotes sister chromatid cohesion through loading and/or maintenance of REC-8, but not COH-3/COH-4, and that the requirement for HTP-3 in REC-8 loading is independent of its role in recruiting HIM-3 or HTP-1/HTP-2 to the axis.

Previous work has indicated that HTP-3 is required for the formation of meiotic DSBs (Goodyer et al., 2008). Thus we examined DSB formation in HTP-3^{6GK} mutants by staining for RAD-51, a DNA strand exchange protein that marks recombination intermediates (Colaiácovo et al., 2003; Sung, 1994). While most germline nuclei in *htp-3* null animals lacked RAD-51 foci, consistent with prior work, RAD-51 foci appeared and disappeared with normal kinetics in HTP-3^{6GK} animals despite the absence of pairing, synapsis, or crossover formation (Figure 6C, S6C). These results indicate that HTP-3's role in DSB formation and/or processing, which has been proposed to involve a direct interaction with the Rad50/Mre11 complex (Goodyer et al., 2008), is also independent of its recruitment of HIM-3 and HTP-1/HTP-2 (Figure 6D). The timely disappearance of RAD-51 foci suggests that axial association of HTP-3 is insufficient to pose a barrier to intersister recombination, consistent with previous evidence that HIM-3 and HTP-1 are required for this barrier in *C. elegans* (Couteau and Zetka, 2005; Couteau et al., 2004).

Meiotic HORMA domain:closure motif interactions are a conserved feature of axis organization

In mouse spermatocytes and oocytes, two meiosis-specific HORMA domain proteins, HORMAD1 and HORMAD2, co-localize on the chromosome axis (Wojtasz et al., 2009). These proteins also physically interact both *in vivo* and *in vitro* (Wojtasz et al., 2012). Like the four *C. elegans* proteins analyzed here, these mammalian proteins contain a HORMA domain followed by a C-terminal tail predicted to lack inherent structure. The tails of mammalian HORMAD1 and HORMAD2 orthologs are highly conserved along their entire lengths, making it impossible to identify putative closure motifs from sequence alone. However, when we compared HORMAD1 to HORMAD2, we noticed two short regions of homology within their tails, including one at their extreme C-termini (Figure 7A), suggesting that this region might mediate protein-protein interactions.

To determine whether HORMAD1 and HORMAD2 might interact in a manner similar to the *C. elegans* HORMA domain proteins, we purified the HORMA domain (residues 2-235 of 394) from human HORMAD1, expressed in *E. coli*. Separately, we expressed and purified the C-terminal tails of HORMAD1 (residues 236-394) and HORMAD2 (residues 245-307), each fused to an N-terminal His_6-maltose binding protein (MBP) tag. In a Ni^{2+} pulldown assay, we found that both full-length tails strongly interacted with HORMAD1(2-235) (Figure 7B, C), suggesting that each tail contains a peptide that can act as a HORMAD1 closure motif. By expressing and purifying tail fragments, we mapped this binding activity to the conserved region at these proteins' C-termini (residues 375-394 of HORMAD1 and 283-307 of HORMAD2). Thus, human HORMAD1 binds a putative closure motif present in the C-terminal tails of both HORMAD1 and HORMAD2 (Figure 7D), indicating that the HORMA domain-tail interactions we have identified in *C. elegans*

are conserved in mammals. It is likely that some details of these interactions differ among lineages, given the variable number of meiotic HORMA proteins and our evidence that mammalian HORMAD1 can bind either its own C-terminus or that of HORMAD2, in contrast to the hierarchical interactions we have documented for the *C. elegans* protein family.

Discussion

Here we report a combined structural and biochemical characterization of the *C. elegans* meiotic HORMA domain proteins, revealing a new mode of interaction at the meiotic chromosome axis. When compared to the well-characterized Mad2 HORMA domain protein, our structures of HIM-3, HTP-1, and HTP-2 show that these proteins adopt a "closed" conformation, with the extended β5-αC loop draping over strands β8′ and β8″ and likely stabilizing the closed state. It is unknown whether the meiotic HORMA domain proteins readily interconvert between "open" and "closed" conformations, as observed for Mad2 (Luo et al., 2000; Sironi et al., 2002). However, we have found that *in vitro*, HIM-3 can bind an HTP-3 closure motif flanked on both ends by a large globular domain, precluding the possibility of this motif "threading" into its binding site (not shown); moreover, HTP-3 tagged at its C-terminus with the globular GFP can function in lieu of wild-type HTP-3 *in vivo*. These observations indicate that HIM-3 and HTP-1/2 must undergo major conformational changes during closure motif binding/exchange. The nature of these changes, as well as their effects on other potential protein-protein interactions within the axis, remain important unanswered questions.

It is highly likely that meiotic HORMA domain proteins engage in additional interactions beyond the HORMA domain:closure motif binding mechanisms we have characterized here. Prior work on Mad2 and Rev7 has shown that the HORMA domain is capable of multiple simultaneous protein-protein interactions, including homodimerization (Hara et al., 2009; Mapelli et al., 2007) and binding of partner proteins along the surface of the extended β-sheet (Kikuchi et al., 2012). Defining the nature of the conformational changes involved in binding/exchange of closure motifs, as well as characterizing interactions with additional potential partners such as cohesins, LAB-1 (de Carvalho et al., 2008), Mre11 (Goodyer et al., 2008), signaling effectors, and/or synaptonemal complex components, will be critical for understanding the central roles played by HORMA domain proteins along meiotic chromosomes. Additionally, identification of effectors specific to HIM-3 or HTP-1/HTP-2 may help explain why these structurally very similar proteins nonetheless play distinct roles at the meiotic chromosome axis.

Meiotic chromosome axis assembly and disassembly are tightly regulated. HORMA domain proteins are detected in the nucleoplasm of proliferating germline nuclei but do not localize to chromosomes, suggesting that their interactions are triggered upon meiotic entry (Burger et al., 2013). Late in meiotic prophase, an early indication of chromosome remodeling and SC disassembly is the restriction of HTP-1/2 to the "long arm" of the chromosomes, while HTP-3 and HIM-3 persist along both arms (Martinez-Perez et al., 2008). We have shown that HTP-1 and HTP-2 can associate with the chromosome axis in two ways: through direct binding to closure motifs in HTP-3 (#1 or #6) or by binding to HIM-3. Our evidence that the

two proteins display distinct binding affinities for these different motifs suggests that there may be differentially regulated pools of HTP-1 and HTP-2 at the chromosome axis. In addition, all of the identified closure motifs contain tyrosine, threonine, and/or serine residues, which may be targets for post-translational modification. Some of these residues lie within consensus phosphorylation motifs for Polo-like or Aurora B kinases, which have been implicated in SC disassembly and regulation of meiotic cohesion in *C. elegans* (Harper et al., 2011; Rogers et al., 2002). We therefore think it likely that dynamic interactions among the HORMA domain proteins are regulated by phosphorylation or other posttranslational modifications within the closure motifs.

An important question for the future is how HTP-3 is recruited to meiotic chromosomes, and whether this recruitment is mediated by interaction of HTP-3's HORMA domain with a closure motif. Our mass spectrometry analysis of chromosome-associated proteins demonstrates that HTP-3 associates with cohesins, suggesting that HTP-3 may bind directly to a cohesin subunit. This hypothesis is consistent with the earlier findings that cohesin complexes are required for HTP-3 recruitment to meiotic chromosomes (Goodyer et al., 2008; Severson et al., 2009). In addition, our evidence demonstrates that the majority of cohesin subunits (most likely COH-3/COH-4-containing cohesin complexes) can associate with chromosomes independently of HTP-3 (Figure 6, S6). Thus, we speculate that cohesins provide a foundation for HTP-3 loading and organization of the meiotic chromosome axis, possibly through HORMA domain-closure motif interactions. Clear functional links between the HORMA domain proteins and cohesin complexes are also observed in other eukaryotes (Klein et al., 1999; Llano et al., 2012; Winters et al., 2014) including mammals, where meiotic chromosome axis structure is disrupted in cohesin mutants (Winters et al., 2014). We therefore propose that HORMA domain proteins may be recruited to the chromosome axis through direct interactions with cohesin subunits in diverse eukaryotic lineages.

How widespread is the hierarchical assembly of HORMA domain proteins that we have outlined in *C. elegans*? The conservation of HIM-3, HTP-1, HTP-2, and HTP-3 orthologs throughout the *Caenorhabditis* genus indicates that the hierarchical assembly mechanism is likely similar within this group, while the variable numbers of closure motifs in HTP-3 orthologs (Figure S1D) may represent lineage-specific optimization of the concentration of HORMA domain proteins along the chromosome axis. Mammals and plants possess two meiotic HORMA domain proteins (HORMAD1/2 and ASY1/2, respectively), while most fungi express only one (Hop1). Our *in vitro* binding results indicate that the HORMA domain-closure motif interactions are conserved in mammals. The apparent lack of specificity/directionality of this interaction suggests that, in mammals, HORMAD1 and HORMAD2 may assemble into a less well-defined hierarchical complex than in *C. elegans*. The highly specific architecture of the *C. elegans* complex may be related to the expansion of this protein family in nematodes, and their additional roles in regulating meiotic cohesion on these organisms' holocentric chromosomes.

While only a single meiotic HORMA domain protein, Hop1, is expressed in most fungi, this protein may nonetheless engage in similar HORMA domain:closure motif interactions. In *Saccharomyces cerevisiae*, initial recruitment of Hop1 to the meiotic chromosome axis

requires its binding partner Red1, but Hop1 function also depends on a short, highly conserved motif at its extreme C-terminus. Disruption of this C-terminal motif by insertions (Friedman et al., 1994) or missense mutations (Niu et al., 2005) strongly affects Hop1 localization and spore viability, and existing evidence is consistent with the idea that it functions as a closure motif. We therefore speculate that Hop1 may be recruited to the axis through multiple mechanisms (*e.g.*, direct binding to DNA, cohesins, and/or Red1, as well as other Hop1 molecules). A hierarchical network of HORMA domain proteins, mediated in part by HORMA domain-closure motif interactions, is likely to be a prominent structural feature of the meiotic chromosome axis throughout eukaryotes.

Experimental Procedures

For full experimental details, see Supplementary Material.

Mass Spectrometry Analysis

C. elegans expressing *htp-3-gfp* (*ieSi6*) were synchronized by bleaching and grown in liquid culture at 20°C until worms reached the young adult stage. Animals were harvested by sucrose flotation, frozen, and disrupted using a mixer mill. HTP-3 complexes (soluble or chromatin-associated) were purified using a GFP-binding protein (Rothbauer et al., 2008). Trypsin-digested samples were analyzed for protein identification by MudPIT (Washburn et al., 2001). To enrich for chromatin-associated proteins, worms were incubated in hypotonic buffer and then homogenized in a dounce homogenizer, then spun at low speed to separate nuclei from cell debris, further purified over a sucrose cushion, then treated with micrococcal nuclease to digest chromatin prior to immunoprecipitation as above.

In vitro reconstitution and peptide binding

ORFs were amplified from a cDNA library and cloned into *E. coli* expression vectors fused to His_6-, His_6-maltose binding protein (MBP), or Strep-tag II sequences (*in vitro* reconstitution). Expressed proteins were purified from bacterial lysates using affinity (Ni^{2+} or Strep), ion-exchange, and size-exclusion chromatography. For crystallization, proteins were concentrated and stored at 4°C, and for biochemical experiments, proteins were aliquoted and frozen at −80°C. Purified samples were characterized by size-exclusion chromatography (Superose 6, GE Life Sciences) and multi-angle light scattering (Wyatt Technologies mini-DAWN Treos) to determine molecular weight and complex stoichiometry. FITC-labeled peptides (BioMatik) at 50 nM were incubated with 12 nM-12.5 μM HORMA protein, fluorescence polarization was read using a TECAN Infinite M1000 PRO fluorescence plate reader, and binding data were analyzed with Graphpad Prism v. 6 using a single-site binding model. For Ni^{2+} pulldown assays, human HORMAD1 was purified as above, and HORMAD1/2 tail sequences were fused to His_6-MBP and purified. Proteins were mixed, then bound to Ni-NTA beads (Qiagen), washed, and bound proteins were visualized by SDS-PAGE.

Crystallization and Structure Solution

Wild-type HIM-3 was purified as above, crystals were grown and cryoprotected in sodium malonate, and the structure was determined using a 2.0 Å resolution single-wavelength

anomalous (SAD) selenomethionine dataset. For crystallization of HIM-3 bound to HTP-3 closure motif #4, residues 277-289 of HIM-3 were replaced by residues 649-663 of HTP-3. For crystallization of HTP-2 complexes, HTP-2 residues 1-253 was co-expressed with a closure motif fused to a TEV protease-cleavable His_6-MBP tag, and complexes purified as above. For crystallization of HTP-1 complexes, HTP-1 residues 1-253, with proline 84 mutated to leucine, was co-expressed with closure motifs as for HTP-2. All HTP-1/HTP-2:closure motif complexes were crystallized and cryoprotected in polyethylene glycol, and structures were solved by SAD or molecular replacement (Table 1).

C. elegans Strains and Immunofluorescence

Strains carrying wild-type, mutant *htp-3-gfp*, and a truncated *him-3* (residues 1-245) transgenes were generated by MosSCI (Frøkjaer-Jensen et al., 2008). Homozygous insertions at the ttTi5605 locus (Chr II) were verified by PCR, and crossed into *htp-3(tm3655)* or *him-3(gk149)* to examine the loading of HORMA domain proteins, cohesin loading and synapsis. Immunofluorescence of dissected gonads was performed as previously described (Phillips et al., 2009).

Supplementary Material

Refer to Web version on PubMed Central for supplementary material.

Acknowledgments

We thank the staffs of NE-CAT beamlines 24ID-C and 24ID-E at the Advanced Photon Source (Argonne, IL), BCSB beamline 8.2.1 at the Advanced Light Source (Berkeley, CA), and beamlines 7-1 and 12-2 at Stanford Synchrotron Light Source (Stanford, CA) for assistance with data collection (see Supplemental Material for synchrotron support statements). We thank Barbara Meyer for providing the anti-SMC-1 antibody, and Lori Kohlstaedt at the UC Berkeley P/MSL for help with mass spectrometry. YK is an HHMI Postdoctoral Fellow of the Damon Runyon Cancer Research Foundation (DRG 2084-11). AFD acknowledges support from the National Institutes of Health (R01 GM065591) and the Howard Hughes Medical Institute, KDC acknowledges support from the Ludwig Institute for Cancer Research, the Sidney Kimmel Foundation Kimmel Scholars program, and the National Institutes of Health (R01 GM104141).

References

Aravind L, Koonin EV. The HORMA domain: a common structural denominator in mitotic checkpoints, chromosome synapsis and DNA repair. Trends Biochem. Sci. 1998; 23:284–286. [PubMed: 9757827]

Baumgartner B, Woltering D, Bagchi S, Larkin B, Loidl J, de los Santos T, Hollingsworth NM. Meiotic segregation, synapsis, and recombination checkpoint functions require physical interaction between the chromosomal proteins Red1p and Hop1p. Mol Cell Biol. 2000; 20:6646–6658. [PubMed: 10958662]

Blat Y, Protacio RU, Hunter N, Kleckner N. Physical and functional interactions among basic chromosome organizational features govern early steps of meiotic chiasma formation. Cell. 2002; 111:791–802. [PubMed: 12526806]

Burger J, Merlet J, Tavernier N, Richaudeau B, Arnold A, Ciosk R, Bowerman B, Pintard L. CRL2(LRR-1) E3-ligase regulates proliferation and progression through meiosis in the *Caenorhabditis elegans* germline. PLoS Genet. 2013; 9:e1003375. [PubMed: 23555289]

Caryl AP, Armstrong SJ, Jones GH, Franklin FC. A homologue of the yeast *HOP1* gene is inactivated in the *Arabidopsis* meiotic mutant *asy1*. Chromosoma. 2000; 109:62–71. [PubMed: 10855496]

Chen Y-T, Venditti CA, Theiler G, Stevenson BJ, Iseli C, Gure AO, Jongeneel CV, Old LJ, Simpson AJG. Identification of CT46/HORMAD1, an immunogenic cancer/testis antigen encoding a putative meiosis-related protein. Cancer Immun. 2005; 5:9. [PubMed: 15999985]

Colaiácovo MP, Macqueen AJ, Martinez-Perez E, McDonald K, Adamo A, La Volpe A, Villeneuve AM. Synaptonemal complex assembly in *C. elegans* is dispensable for loading strand-exchange proteins but critical for proper completion of recombination. Dev Cell. 2003; 5:463–474. [PubMed: 12967565]

Couteau F, Zetka M. HTP-1 coordinates synaptonemal complex assembly with homolog alignment during meiosis in *C. elegans*. Genes Dev. 2005; 19:2744–2756. [PubMed: 16291647]

Couteau F, Zetka M. DNA Damage during Meiosis Induces Chromatin Remodeling and Synaptonemal Complex Disassembly. Dev Cell. 2011; 20:353–363. [PubMed: 21397846]

Couteau F, Nabeshima K, Villeneuve A, Zetka M. A component of *C. elegans* meiotic chromosome axes at the interface of homolog alignment, synapsis, nuclear reorganization, and recombination. Curr. Biol. 2004; 14:585–592. [PubMed: 15062099]

Daniel K, Lange J, Hached K, Fu J, Anastassiadis K, Roig I, Cooke HJ, Stewart AF, Wassmann K, Jasin M, et al. Meiotic homologue alignment and its quality surveillance are controlled by mouse HORMAD1. Nat. Cell Biol. 2011; 13:599–610. [PubMed: 21478856]

de Carvalho CE, Zaaijer S, Smolikov S, Gu Y, Schumacher JM, Colaiácovo MP. LAB-1 antagonizes the Aurora B kinase in *C. elegans*. Genes Dev. 2008; 22:2869–2885. [PubMed: 18923084]

Friedman DB, Hollingsworth NM, Byers B. Insertional mutations in the yeast *HOP1* gene: evidence for multimeric assembly in meiosis. Genetics. 1994; 136:449–464. [PubMed: 8150275]

Frøkjaer-Jensen C, Davis MW, Hopkins CE, Newman BJ, Thummel JM, Olesen S-P, Grunnet M, Jorgensen EM. Single-copy insertion of transgenes in *Caenorhabditis elegans*. Nat Genet. 2008; 40:1375–1383. [PubMed: 18953339]

Fukuda T, Daniel K, Wojtasz L, Toth A, Höög C. A novel mammalian HORMA domain-containing protein, HORMAD1, preferentially associates with unsynapsed meiotic chromosomes. Exp Cell Res. 2010; 316:158–171. [PubMed: 19686734]

Goodyer W, Kaitna S, Couteau F, Ward JD, Boulton SJ, Zetka M. HTP-3 links DSB formation with homolog pairing and crossing over during *C. elegans* meiosis. Dev Cell. 2008; 14:263–274. [PubMed: 18267094]

Hara K, Hashimoto H, Murakumo Y, Kobayashi S, Kogame T, Unzai S, Akashi S, Takeda S, Shimizu T, Sato M. Crystal structure of human REV7 in complex with a human REV3 fragment and structural implication of the interaction between DNA polymerase zeta and REV1. J Biol Chem. 2010; 285:12299–12307. [PubMed: 20164194]

Hara K, Shimizu T, Unzai S, Akashi S, Sato M, Hashimoto H. Purification, crystallization and initial X-ray diffraction study of human REV7 in complex with a REV3 fragment. Acta Crystallogr. Sect. F Struct. Biol. Cryst. Commun. 2009; 65:1302–1305.

Harper NC, Rillo R, Jover-Gil S, Assaf ZJ, Bhalla N, Dernburg AF. Pairing centers recruit a Polo-like kinase to orchestrate meiotic chromosome dynamics in *C. elegans*. Dev Cell. 2011; 21:934–947. [PubMed: 22018922]

Hodgkin J, Horvitz HR, Brenner S. Nondisjunction Mutants of the Nematode *CAENORHABDITIS ELEGANS*. Genetics. 1979; 91:67–94. [PubMed: 17248881]

Hollingsworth NM, Johnson AD. A conditional allele of the *Saccharomyces cerevisiae HOP1* gene is suppressed by overexpression of two other meiosis-specific genes: *RED1* and *REC104*. Genetics. 1993; 133:785–797. [PubMed: 8462842]

Hollingsworth NM, Goetsch L, Byers B. The *HOP1* gene encodes a meiosis-specific component of yeast chromosomes. Cell. 1990; 61:73–84. [PubMed: 2107981]

Jao CC, Ragusa MJ, Stanley RE, Hurley JH. A HORMA domain in Atg13 mediates PI 3-kinase recruitment in autophagy. Proc. Natl. Acad. Sci. USA. 2013; 110:5486–5491. [PubMed: 23509291]

Kaitna S, Pasierbek P, Jantsch M, Loidl J, Glotzer M. The aurora B kinase AIR-2 regulates kinetochores during mitosis and is required for separation of homologous Chromosomes during meiosis. Curr. Biol. 2002; 12:798–812. [PubMed: 12015116]

Karplus PA, Diederichs K. Linking crystallographic model and data quality. Science. 2012; 336:1030–1033. [PubMed: 22628654]

Kikuchi S, Hara K, Shimizu T, Sato M, Hashimoto H. Structural basis of recruitment of DNA polymerase ζ by interaction between REV1 and REV7 proteins. J Biol Chem. 2012; 287:33847–33852. [PubMed: 22859296]

Kleckner N. Chiasma formation: chromatin/axis interplay and the role(s) of the synaptonemal complex. Chromosoma. 2006; 115:175–194. [PubMed: 16555016]

Klein F, Mahr P, Gálová M, Buonomo SB, Michaelis C, Nairz K, Nasmyth K. A central role for cohesins in sister chromatid cohesion, formation of axial elements, and recombination during yeast meiosis. Cell. 1999; 98:91–103. [PubMed: 10412984]

Llano E, Herrán Y, García-Tuñón I, Gutiérrez-Caballero C, de Álava E, Barbero JL, Schimenti J, de Rooij DG, Sánchez-Martín M, Pendás AM. Meiotic cohesin complexes are essential for the formation of the axial element in mice. J Cell Biol. 2012; 197:877–885. [PubMed: 22711701]

Luo X, Fang G, Coldiron M, Lin Y, Yu H, Kirschner MW, Wagner G. Structure of the Mad2 spindle assembly checkpoint protein and its interaction with Cdc20. Nat. Struct. Biol. 2000; 7:224–229. [PubMed: 10700282]

Luo X, Tang Z, Rizo J, Yu H. The Mad2 spindle checkpoint protein undergoes similar major conformational changes upon binding to either Mad1 or Cdc20. Mol Cell. 2002; 9:59–71. [PubMed: 11804586]

Luo X, Tang Z, Xia G, Wassmann K, Matsumoto T, Rizo J, Yu H. The Mad2 spindle checkpoint protein has two distinct natively folded states. Nat Struct Mol Biol. 2004; 11:338–345. [PubMed: 15024386]

Mapelli M, Massimiliano L, Santaguida S, Musacchio A. The Mad2 Conformational Dimer: Structure and Implications for the Spindle Assembly Checkpoint. Cell. 2007; 131:730–743. [PubMed: 18022367]

Martinez-Perez E, Villeneuve AM. HTP-1-dependent constraints coordinate homolog pairing and synapsis and promote chiasma formation during *C. elegans* meiosis. Genes Dev. 2005; 19:2727–2743. [PubMed: 16291646]

Martinez-Perez E, Schvarzstein M, Barroso C, Lightfoot J, Dernburg AF, Villeneuve AM. Crossovers trigger a remodeling of meiotic chromosome axis composition that is linked to two-step loss of sister chromatid cohesion. Genes Dev. 2008; 22:2886–2901. [PubMed: 18923085]

Nabeshima K, Villeneuve AM, Colaiácovo MP. Crossing over is coupled to late meiotic prophase bivalent differentiation through asymmetric disassembly of the SC. J Cell Biol. 2005; 168:683–689. [PubMed: 15738262]

Niu H, Wan L, Baumgartner B, Schaefer D, Loidl J, Hollingsworth NM. Partner choice during meiosis is regulated by Hop1-promoted dimerization of Mek1. Mol Biol Cell. 2005; 16:5804–5818. [PubMed: 16221890]

Orth M, Mayer B, Rehm K, Rothweiler U, Heidmann D, Holak TA, Stemmann O. Shugoshin is a Mad1/Cdc20-like interactor of Mad2. Embo J. 2011; 30:2868–2880. [PubMed: 21666598]

Pangas SA, Yan W, Matzuk MM, Rajkovic A. Restricted germ cell expression of a gene encoding a novel mammalian HORMA domain-containing protein. Gene Expr. Patterns. 2004; 5:257–263. [PubMed: 15567723]

Panizza S, Mendoza MA, Berlinger M, Huang L, Nicolas A, Shirahige K, Klein F. Spo11-accessory proteins link double-strand break sites to the chromosome axis in early meiotic recombination. Cell. 2011; 146:372–383. [PubMed: 21816273]

Pasierbek P, Jantsch M, Melcher M, Schleiffer A, Schweizer D, Loidl J. A *Caenorhabditis elegans* cohesion protein with functions in meiotic chromosome pairing and disjunction. Genes Dev. 2001; 15:1349–1360. [PubMed: 11390355]

Phillips CM, McDonald KL, Dernburg AF. Cytological analysis of meiosis in Caenorhabditis elegans. Methods Mol Biol. 2009; 558:171–195. [PubMed: 19685325]

Rogers E, Bishop JD, Waddle JA, Schumacher JM, Lin R. The aurora kinase AIR-2 functions in the release of chromosome cohesion in *Caenorhabditis elegans* meiosis. J Cell Biol. 2002; 157:219–229. [PubMed: 11940606]

Rothbauer U, Zolghadr K, Muyldermans S, Schepers A, Cardoso MC, Leonhardt H. A versatile nanotrap for biochemical and functional studies with fluorescent fusion proteins. Mol. Cell Proteomics. 2008; 7:282–289. [PubMed: 17951627]

Schwacha A, Kleckner N. Interhomolog bias during meiotic recombination: meiotic functions promote a highly differentiated interhomolog-only pathway. Cell. 1997; 90:1123–1135. [PubMed: 9323140]

Severson AF, Ling L, van Zuylen V, Meyer BJ. The axial element protein HTP-3 promotes cohesin loading and meiotic axis assembly in *C. elegans* to implement the meiotic program of chromosome segregation. Genes Dev. 2009; 23:1763–1778. [PubMed: 19574299]

Shin Y-H, Choi Y, Erdin SU, Yatsenko SA, Kloc M, Yang F, Wang PJ, Meistrich ML, Rajkovic A. *Hormad1* mutation disrupts synaptonemal complex formation, recombination, and chromosome segregation in mammalian meiosis. PLoS Genet. 2010; 6:e1001190. [PubMed: 21079677]

Sironi L, Mapelli M, Knapp S, de Antoni A, Jeang K-T, Musacchio A. Crystal structure of the tetrameric Mad1-Mad2 core complex: implications of a “safety belt” binding mechanism for the spindle checkpoint. Embo J. 2002; 21:2496–2506. [PubMed: 12006501]

Sung P. Catalysis of ATP-dependent homologous DNA pairing and strand exchange by yeast RAD51 protein. Science. 1994; 265:1241–1243. [PubMed: 8066464]

Tzur YB, Egydio de Carvalho C, Nadarajan S, Van Bostelen I, Gu Y, Chu DS, Cheeseman IM, Colaiácovo MP. LAB-1 targets PP1 and restricts Aurora B kinase upon entrance into meiosis to promote sister chromatid cohesion. PLoS Biol. 2012; 10:e1001378. [PubMed: 22927794]

Washburn MP, Wolters D, Yates JR. Large-scale analysis of the yeast proteome by multidimensional protein identification technology. Nat. Biotechnol. 2001; 19:242–247. [PubMed: 11231557]

Winters T, McNicoll F, Jessberger R. Meiotic cohesin STAG3 is required for chromosome axis formation and sister chromatid cohesion. Embo J. 2014; 33:1256–1270. [PubMed: 24797474]

Wojtasz L, Cloutier JM, Baumann M, Daniel K, Varga J, Fu J, Anastassiadis K, Stewart AF, Reményi A, Turner JMA, et al. Meiotic DNA double-strand breaks and chromosome asynapsis in mice are monitored by distinct HORMAD2-independent and - dependent mechanisms. Genes Dev. 2012; 26:958–973. [PubMed: 22549958]

Wojtasz L, Daniel K, Roig I, Bolcun-Filas E, Xu H, Boonsanay V, Eckmann CR, Cooke HJ, Jasin M, Keeney S, et al. Mouse HORMAD1 and HORMAD2, two conserved meiotic chromosomal proteins, are depleted from synapsed chromosome axes with the help of TRIP13 AAA-ATPase. PLoS Genet. 2009; 5:e1000702. [PubMed: 19851446]

Xia G, Luo X, Habu T, Rizo J, Matsumoto T, Yu H. Conformation-specific binding of p31(comet) antagonizes the function of Mad2 in the spindle checkpoint. Embo J. 2004; 23:3133–3143. [PubMed: 15257285]

Yang M, Li B, Tomchick DR, Machius M, Rizo J, Yu H, Luo X. p31comet blocks Mad2 activation through structural mimicry. Cell. 2007; 131:744–755. [PubMed: 18022368]

Zetka MC, Kawasaki I, Strome S, Müller F. Synapsis and chiasma formation in *Caenorhabditis elegans* require HIM-3, a meiotic chromosome core component that functions in chromosome segregation. Genes Dev. 1999; 13:2258–2270. [PubMed: 10485848]

Zickler D, Kleckner N. Meiotic chromosomes: integrating structure and function. Annu Rev Genet. 1999; 33:603–754. [PubMed: 10690419]

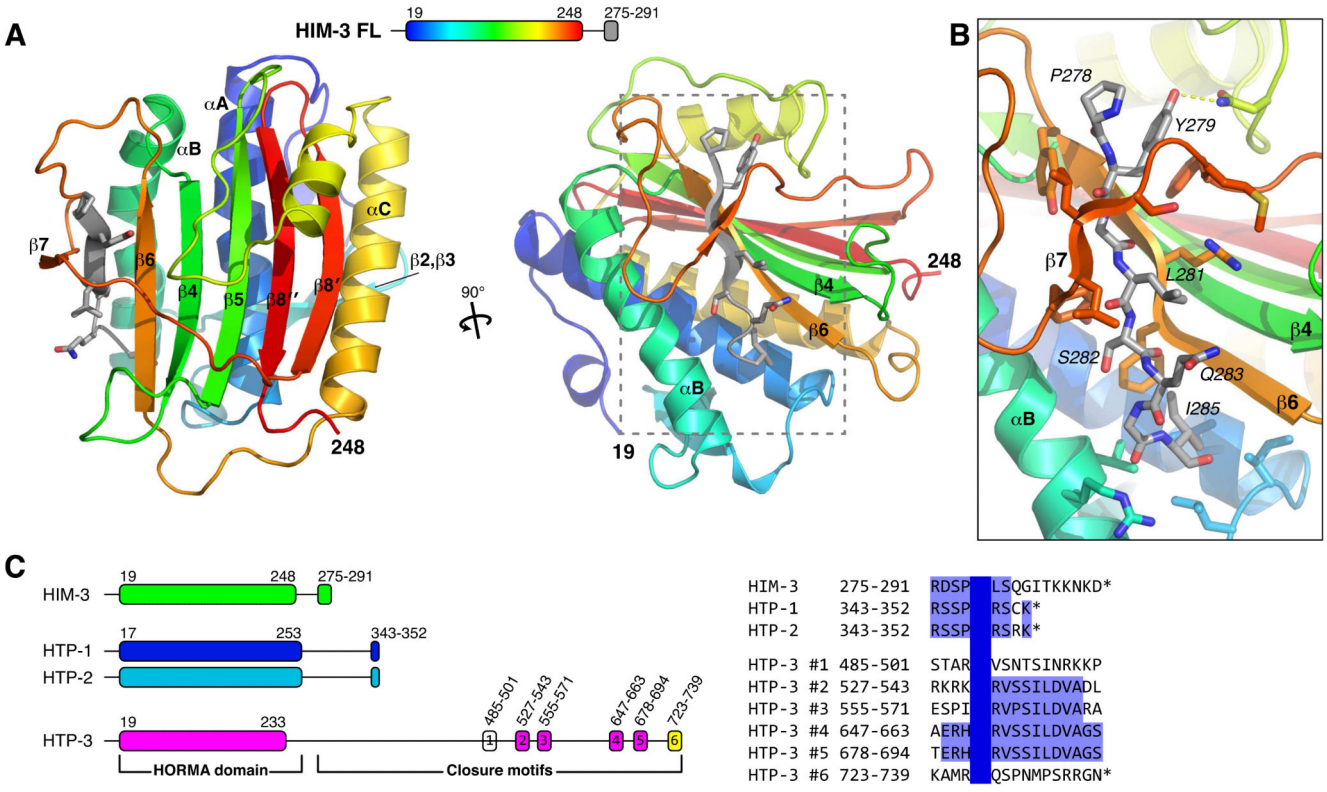

Figure 1. Structure of *C. elegans* HIM-3 reveals conserved "closure motifs"

(A) Two views of *C. elegans* HIM-3, with HORMA domain colored as a rainbow from N- to C-termini and secondary structure elements labeled according to the Mad2 convention (Luo et al., 2002; Sironi et al., 2002), with the C-terminal "closure motif" residues 278-285 in gray (see schematic, top). See Figure S1A for comparison with Mad2 and Rev7. (B) Detail view showing interactions between the closure motif and the "safety belt" of HIM-3. (C) Left: schematic of HIM-3, HTP-1, HTP-2 and HTP-3 N-terminal HORMA domains and C-terminal "closure motifs." Right: alignment of putative closure motifs from all four *C. elegans* HORMA domain proteins. See also Figure S1B-D.

A **HTP-3-GFP Mass Spectrometry Analysis**

Locus	Gene name	Size (kDa)	Sequence coverage (%) Soluble	Chromatin	Note
ZK381.1	*him-3*	33.1	41.9	41.9	HORMA
F41H10.10	*htp-1*	39.6	23.6	24.7	HORMA
Y73B6BL.2	*htp-2*	39.6	30.1	12.2	HORMA
F57C9.5	*htp-3*	81.6	9.1	12.4	HORMA
Y47D3A.26	*smc-3*	139.9	-	10.0	Smc3
F28B3.7a	*him-1*	144.2	-	9.2	Smc1
F08H9.1	*coh-3*	70.4	-	4.1	meiotic kleisin
Y45G5AM.8	*coh-4*	70.5	-	8.9	meiotic kleisin
W02A2.6	*rec-8*	89.9	-	3.7	meiotic kleisin
H38K22.1	*evl-14*	177.9	-	2.0	Pds5

B **Size Exclusion Chromatography**

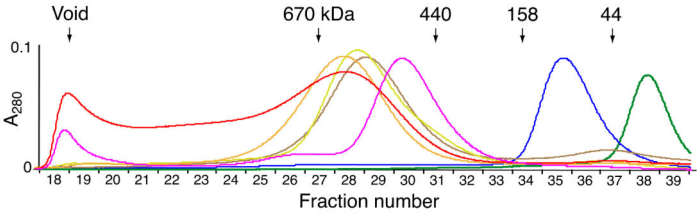

Protein/Complex	Measured MW (kDa)	Predicted MW (kDa)	Stoichiometry
HIM-3	29.7	33.1	monomer
HTP-3	81.4	81.6	monomer
HTP-1:HIM-3	70.8	72.7	1:1
HTP-1 (1-253):HIM-3	60.3	64.3	1:1
HTP-3:HIM-3	140 -180[a]	151.3 -185.2	1:2 -1:3
HTP-3:HTP-1	158	164.3	1:2
HTP-3:HTP-1:HIM-3	200 -330[a]		variable
HTP-3:HTP-1:HTP-2:HIM-3	300 -400[a]		variable

C

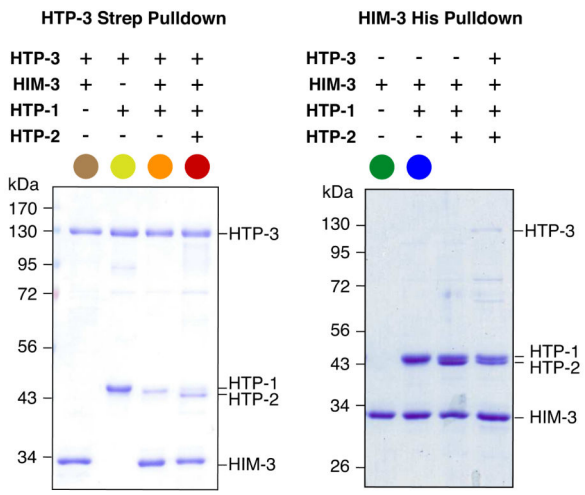

Figure 2. The *C. elegans* meiotic HORMA domain proteins form a complex

(A) Mass spectrometry results from HTP-3-GFP pulldowns. Pulldowns were performed in conditions that favored either soluble or chromatin-associated complexes (see Extended Experimental Procedures). (B) Size exclusion chromatography and multi-angle light scattering (SEC-MALS) analysis of HORMA domain protein complexes (a: complexes containing HTP-3 showed strong polydispersity indicative of a mixture of different-weight particles). See Figure S2 for SDS-PAGE analysis of fractions and representative SEC-MALS results. (C) SDS-PAGE analysis of co-expressed complexes purified using Strep-HTP-3 (left panel) or HIM-3-6His (right panel).

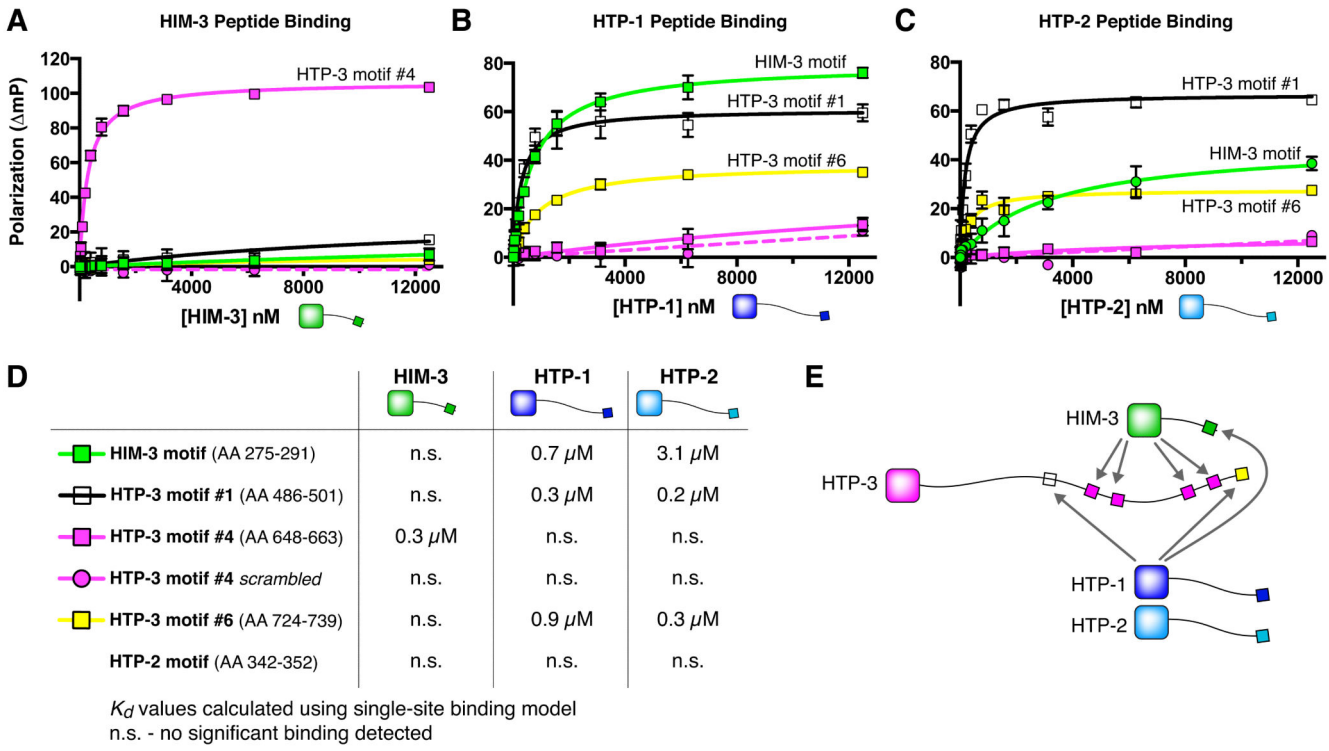

Figure 3. *C. elegans* HORMA domain proteins bind distinct closure motifs

(A-C) Fluorescence polarization (FP) peptide-binding assay for HIM-3 (A), HTP-1 (B), and HTP-2 (C). Peptides used are shown in panel (D). (D) Measured K_d's for HIM-3, HTP-1, and HTP-2 binding different closure motifs. n.s.; no significant binding detected. (E) Schematic illustrating the closure motif binding specificities of HIM-3, HTP-1, and HTP-2.

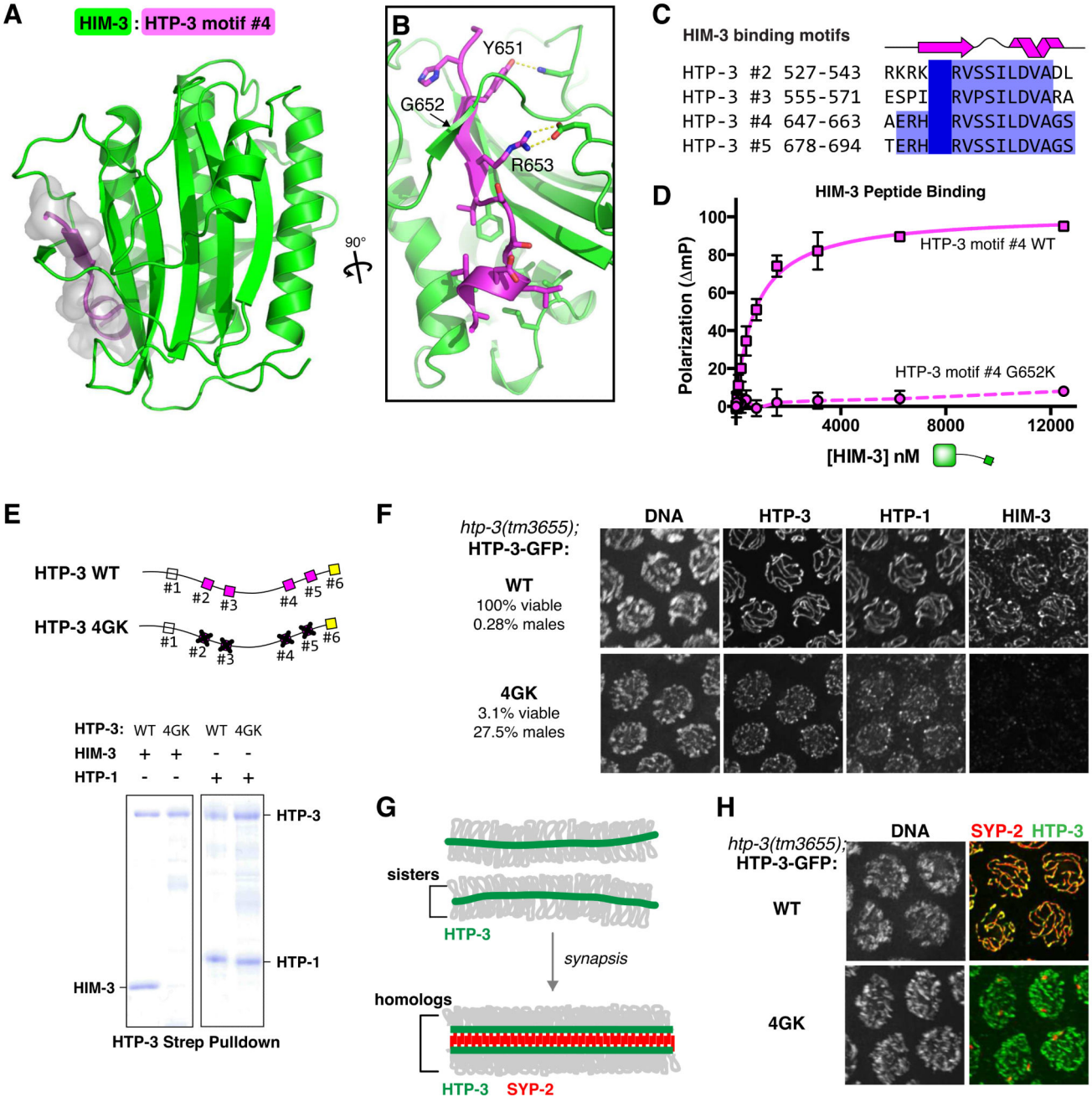

Figure 4. HIM-3 binding to HTP-3 motifs #2-5 is critical for homolog synapsis and successful meiosis

(A) Structure of HIM-3 (green) bound to HTP-3 motif #4 (magenta). Molecular surface is shown in gray for the bound closure motif. (B) Detail view showing interactions between the closure motif and the "safety belt" of HIM-3. See also Figure S3. (C) Sequence alignment of HTP-3 motifs #2-#5. (D) FP peptide binding assay for HIM-3 binding HTP-3 motif #4 wild-type (as in Figure 3A) and G652K mutant. See also Figure S4. (E) Strep-tagged HTP-3, either wild-type or 4GK mutant (conserved glycine in HTP-3 motifs #2-#5 mutated to lysine; schematic at top), was coexpressed in *E. coli* with untagged HIM-3 (*left*) or HTP-1

(*right*), and purified using Strep-tactin resin to isolate HTP-3 and directly bound proteins. (F) Wild-type and 4GK mutant *htp-3-gfp* transgenes were expressed in the *htp-3(tm3655)I* background, and mid-pachytene nuclei stained for DNA, HTP-3:GFP, HTP-1, and HIM-3. Scale bar, 5 μm. (G) Schematic showing meiotic chromosome axis formation and synapsis. (H) Wild-type or 4GK mutant HTP-3:GFP transgenes were expressed in the *htp-3(tm3655)I* background, and mid-pachytene nuclei were stained for DNA, HTP-3:GFP (green), and SYP-2 (red). All images are maximum-intensity projections of deconvolved 3D image stacks. Scale bar, 5 μm. See also Figure S5.

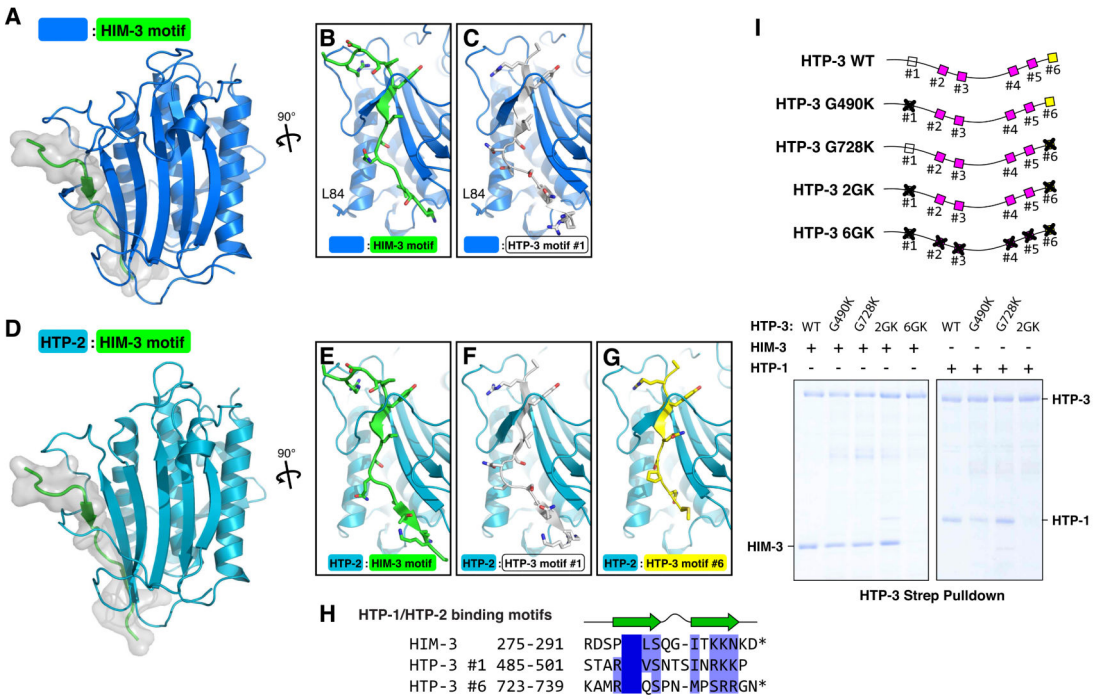

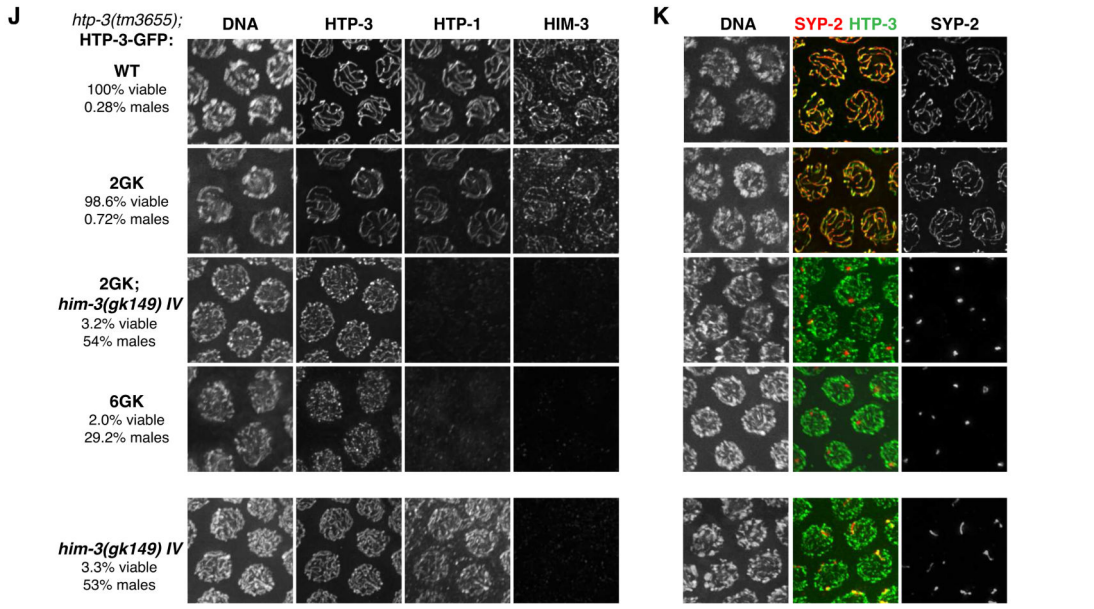

Figure 5. HTP-1/HTP-2 is recruited to chromosomes by both HTP-3 and HIM-3

(A) Structure of HTP-1^{P84L} (blue) bound to the HIM-3 closure motif (green). A molecular surface representation is shown in gray for the bound closure motif. (B-C) Detail views showing interactions between HTP-1^{P84L} and the HIM-3 closure motif (B) or HTP-3 motif #1 (C). Leucine 84 is shown in stick view. See Figure S3 for representative electron density. (D) Structure of HTP-2 (cyan) bound to the HIM-3 closure motif (green). (E-G) Detail views showing interactions between HTP-2 and the HIM-3 closure motif (E), HTP-3 motif #1 (F), or HTP-3 motif #6 (G). (H) Sequence alignment of closure motifs specific for

binding the HTP-1 and HTP-2 HORMA domains. (I) Strep-tagged HTP-3 wild-type or GK mutants (schematic at top) were coexpressed in *E. coli* with untagged HIM-3 (*left*) or HTP-1 (*right*), and purified using Strep-tactin resin to isolate HTP-3 and directly bound proteins. (J) Wild-type, 2GK, and 6GK mutant *htp-3-gfp* transgenes were expressed in the *htp-3(tm3655)I* background and combined with the *him-3(gk149) IV* null allele, and mid-pachytene nuclei stained for DNA, HTP-3:GFP, HTP-1, and HIM-3. Scale bar, 5 μm. (K) Projection images showing mid-pachytene nuclei of the strains in (J) stained for DNA, HTP-3:GFP (green), and SYP-2 (red). Scale bar, 5 μm. See also Figure S5.

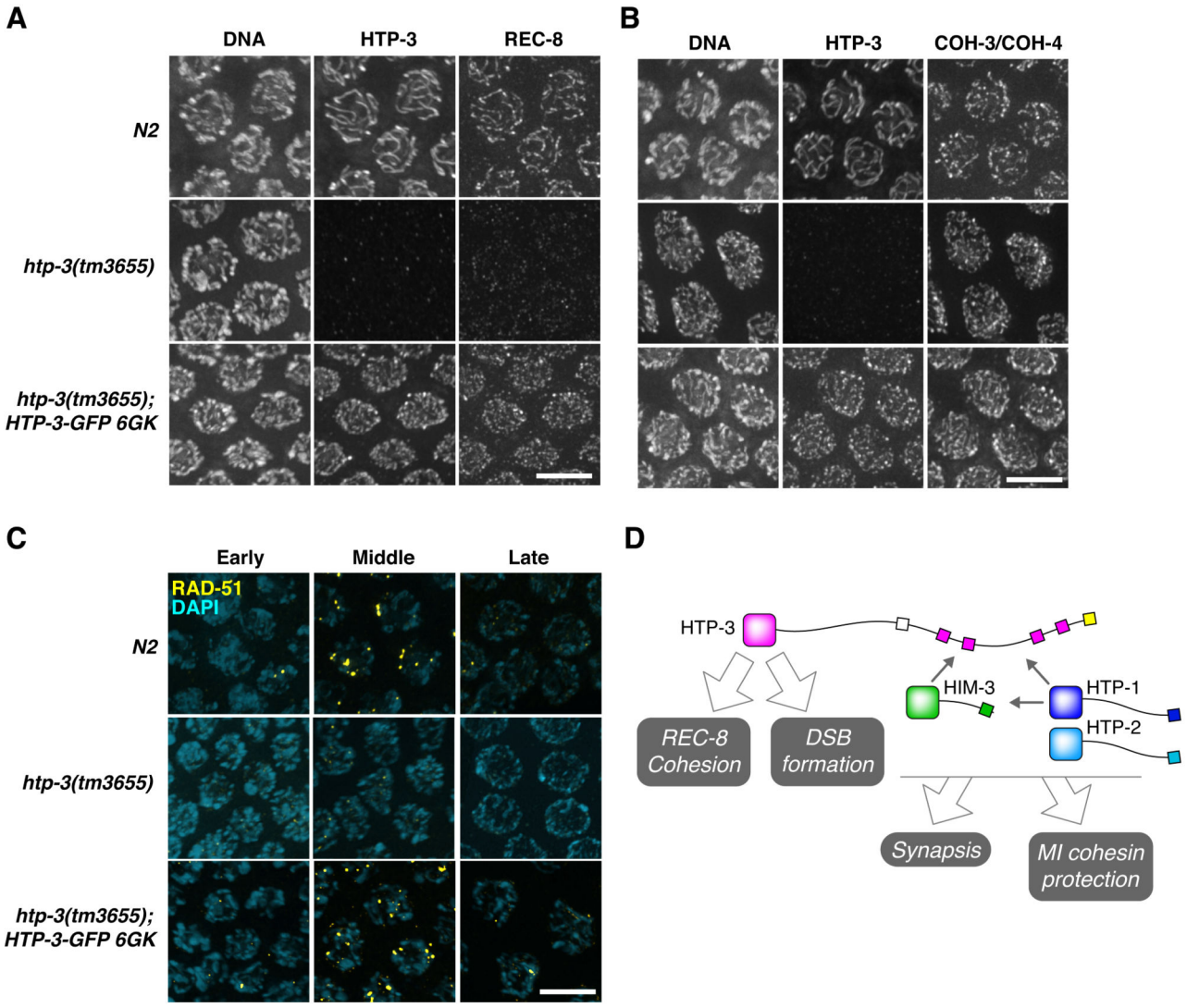

Figure 6. Chromosome axis localization of cohesin complexes in HTP-3 closure motif GK mutants

(A) and (B) Mid-pachytene nuclei in wild-type *N2*, *htp-3*(*tm3655*), and *htp-3(tm3655);htp-3*^{6GK} worms were stained for HTP-3 and meiosis-specific kleisin subunits of the cohesin complex, REC-8 (A) or COH-3/COH-4 (B). Scale bar, 5 μm. See Figure S6 for localization of SMC subunits SMC-1 and SMC-3. (C) Projection images showing mid-pachytene nuclei stained for DNA and RAD-51 to assess the formation and repair of meiotic DSBs. (D) Schematic illustrating the major functions and proposed roles of the *C. elegans* meiotic HORMA domain proteins.

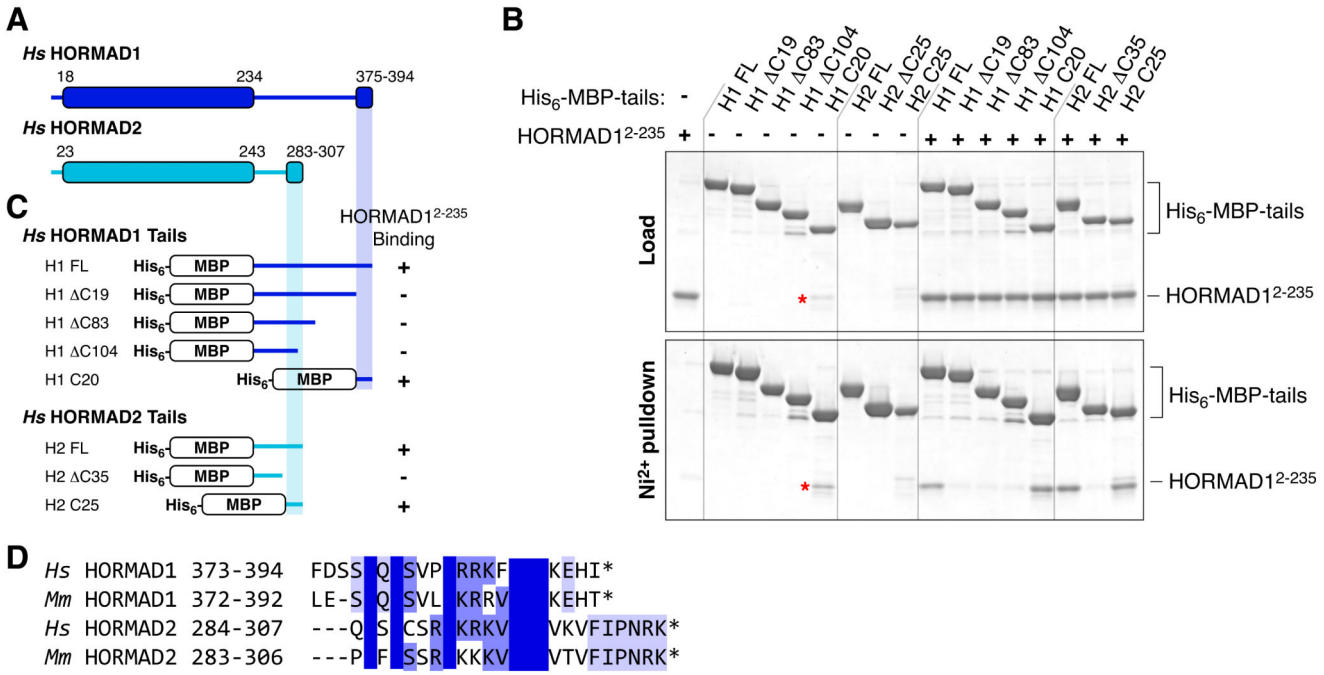

Figure 7. Mammalian HORMAD1 and HORMAD2 contain C-terminal closure motifs

(A) Schematic of human HORMAD1 and HORMAD2, with HORMA domain and C-terminal region shown as boxes. (B) Ni^{2+} pulldown using His_6-MBP-tagged HORMAD1/2 tail segments, with untagged human HORMAD1(2-235) as prey. *Top panel*: 10% Load sample, *Bottom panel*: Ni^{2+}-bound fraction. Red asterisks (*) indicate a contaminant in the HORMAD1 ΔC104 tail construct that is of similar molecular weight to HORMAD1(2-235). (C) Schematic of results from (B), showing that the extreme C-terminal regions of both HORMAD1 and HORMAD2 are necessary and sufficient for HORMAD1(2-235) binding. (D) Sequence alignment of putative HORMAD1 and HORMAD2 closure motifs from human (*Hs*) and mouse (*Mm*).

Table 1

Data Collection and Refinement Statistics

Data collection	**HIM-3 (SeMet)**	**HIM-3 Native**	**HIM-3: HTP-3 motif #4**	**HTP-2:HIM-3 motif $P2_12_12_1$ SeMet**	**HTP-2:HIM-3 motif $P2_12_12_1$ Native**	**HTP-2:HIM-3 motif $P2_1$**	**HTP-2: HTP-3 motif #1**	**HTP-2: HTP-3 motif #6**	**HTP-1^{P84L}: HIM-3 motif**	**HTP-1^{P84L}: HTP-3 motif #1**
Synchrotron/Beamline	APS 24ID-E	APS 24ID-E	SSRL 12-2	ALS 8.2.1	SSRL 12-2	ALS 8.2.1	ALS 8.2.1	APS 24 ID-E	APS 24 ID-E	SSRL 7-1
Resolution (Å)	50.0 – 2.00	50.0 – 1.75	40 – 2.85	50 – 3.4	40 – 2.55	50 – 2.55	30 – 2.30	80 – (3.4/3.1)[g]	50 – 2.4	50 – 2.3
Wavelength (Å)	0.979	0.979	0.979	0.979	0.979	0.984	1.000	0.979	0.979	0.979
Space Group	$P6_1$	$P6_1$	R32	$P2_12_12_1$	$P2_12_12_1$	$P2_1$	$P2_1$	C2	$P2_1$	$P2_1$
Unit Cell Dimensions (a, b, c) Å	73.19, 73.19, 110.44	73.14, 73.14, 110.45	161.791, 161.79, 110.55	66.80, 81.84, 118.79	66.23, 82.67, 118.70	46.75, 65.69, 93.69	47.68, 66.01, 94.65	165.82, 38.31, 103.82	66.90, 107.87, 82.97	53.07, 66.4, 84.13
Unit cell Angles (α,β,γ) °	90, 90, 120	90, 90, 120	90, 90, 120	90, 90, 90	90, 90, 90	90, 90.70, 90	90, 90.27, 90	90, 126.24, 90	90, 90.104, 90	90, 105.578, 90
I/σ (last shell)	17.3 (2.4)	13.2 (1.4)	20.1 (1.4)	7.9 (2.0)	15.8 (1.4)	21.4 (1.6)	14.5 (1.9)	8.7 (2.0)	6.3 (1.2)	14.2 (4.3)
[a] R_{sym} (last shell)	0.092 (0.726)	0.123 (1.457)	0.057 (1.361)	0.176 (0.779)	0.087 (1.631)	0.085 (0.923)	0.107 (0.469)	0.132 (0.601)	0.132 (0.647)	0.073 (0.282)
[b] R_{meas} (last shell)	0.131 (0.865)	0.133 (1.571)	0.062 (1.469)	0.214 (0.951)	0.095 (1.769)	0.122 (>1.0)	0.129 (0.593)	0.156 (0.735)	0.175 (0.863)	0.087 (0.338)
[c] $CC_{1/2}$, last shell	0.738	0.454	0.656	0.628	0.745	0.654	0.836	0.739	0.591	0.906
Completeness (last shell) %	100.0 (99.9)	100.0 (99.9)	95.7 (96.5)	95.9 (96.7)	99.0 (98.2)	100.0 (99.8)	93.8 (72.9)[f]	83.4 (10.0)[f]	94.1 (93.6)	97.3 (94.8)
Number of reflections	167813	254169	87887	49601	143932	106465	81630	29834	86305	87584
unique	22367	33729	12444	16424	21690	18895	24989	8218	43476	24480
Multiplicity (last shell)	7.5 (6.9)	7.5 (7.2)	7.1 (7.2)	3.0 (3.0)	6.6 (6.6)	5.6 (5.3)	3.3 (2.3)	3.6 (2.8)	2.0 (2.0)	3.6 (3.3)
Number of sites	5	-	-	12	-	-	-	-	-	-
Refinement										
Resolution (Å)		50.0 – 1.75	50 – 2.85		40 – 2.55	50 – 2.55	30 – 2.30	83 – 3.10	50 – 2.4	50 – 2.3
No. of reflections		33673	12376		21562	18858	24692	8216	43408	24368
free		1705	580		1083	977	1269	377	2203	1163
[d] R_{work} (last shell) %		15.82 (30.07)	17.79 (29.68)		22.85 (45.59)	19.61 (27.24)	20.29 (27.25)	28.01 (35.73)	24.57 (32.72)	24.11 (24.22)
[d] R_{free} (last shell) %		18.53 (37.95)	22.99 (31.88)		26.42 (44.67)	23.00 (34.01)	21.64 (33.92)	31.98 (35.59)	28.22 (34.77)	27.93 (28.85)
Structure/Stereochemistry										
No. of atoms		4121	1923		3932	3896	3944	3815	8235	4153
solvent		287	0		18	41	56	0	283	196

Dev Cell. Author manuscript; available in PMC 2015 November 24.

Data collection	HIM-3 (SeMet)	HIM-3 Native	HIM-3: HTP-3 motif #4	HTP-2:HIM-3 motif $P2_12_12_1$ SeMet	HTP-2:HIM-3 motif $P2_12_12_1$ Native	HTP-2:HIM-3 motif $P2_1$	HTP-2: HTP-3 motif #1	HTP-2: HTP-3 motif #6	HTP-1^{P84L}: HIM-3 motif	HTP-1^{P84L}: HTP-3 motif #1
r.m.s.d. bond lengths (Å)		0.011	0.004		0.004	0.002	0.003	0.003	0.004	0.003
r.m.s.d. bond angles (°)		1.224	0.839		0.771	0.570	0.647	0.604	0.770	0.768
[e] Protein Data Bank ID	N/A	4TRK	4TZJ	N/A	4TZL	4TZS	4TZM	4TZN	4TZO	4TZQ

[a] $R_{sym} = \Sigma\Sigma_j|I_j - \langle I\rangle|/\Sigma I_j$, where I_j is the intensity measurement for reflection j and $\langle I\rangle$ is the mean intensity for multiply recorded reflections.

[b] $R_{meas} = \Sigma h\,[\sqrt{(n/(n-1))}\,\Sigma_j\,[I_{hj} - \langle I_h\rangle]\,/\,\Sigma_{hj}\,\langle I_h\rangle$, where I_{hj} is a single intensity measurement for reflection h, $\langle I_h\rangle$ is the average intensity measurement for multiply recorded reflections, and n is the number of observations of reflection h.

[c] $CC_{1/2}$ is the Pearson correlation coefficient between the average measured intensities of two randomly-assigned half-sets of the measurements of each unique reflection (Karplus and Diederichs, 2012).

[d] $R_{work,\ free} = \Sigma||F_{obs}| - |F_{calc}||/|F_{obs}|$, calculated using the working and free reflection sets, respectively.

[e] Coordinates and structure factors are deposited with the Protein Data Bank (http://www.pdb.org).

[f] Data were highly anisotropic, leading to systematic data incompleteness.

[g] Data were scaled using anisotropic resolution cutoffs; 3.4 Å along the a and c axes, 3.1 Å along the b axis.